Macromolecules
ARTICLE

Macromolecules **2009**, *42*, 4787–4794 **4787**
DOI: 10.1021/ma9002616

Self-Assembling Microporous Matrix from Dendritic−Linear Copolymers Based on a Solvent-Induced Phase Separation Mechanism

Shang-Ju Hsieh,[1] Cheng-Chien Wang,[2] and Chuh-Yung Chen*,[1]

[1]*Department of Chemical Engineering, National Cheng Kung University, 70101, Tainan, Taiwan, and*
[2]*Department of Chemical and Materials Engineering, Southern Taiwan University, 710, Tainan, Taiwan*

Received February 5, 2009; Revised Manuscript Received May 12, 2009

ABSTRACT: A set of dendritic−linear copolymers, poly(glycidyl methacrylate-grafted-dimethyl 3,3′-(4-hydroxyphenylazanediyl)bis(2-methylpropanoate))-*random*-polystyrene (PGMA-HPAM-*r*-PS), were successfully prepared by copolymerization of the novel dendritic macromonomer dimethyl 3,3′-(4-(2-hydroxy-3-(methacryloyloxy)propoxy)phenylazanediyl)bis(2-methylpropanoate) (GMA-HPAM) and a styrene monomer. The dendritic GMA-HPAM macromonomer dendron 3,3′-(4-hydroxyphenylazanediyl) bis(*N*-(2-aminoethyl)-2-methylpropanamide) (HPAM) was then grafted using the divergent growth method. ^{1}H NMR and ^{13}C NMR spectra were used to identify the structure of the dendritic−linear GMA-HPAM-*r*-PS copolymer. Microporous dendritic−linear PGMA-HPAM-*r*-PS copolymer films in this system were prepared by using solvent-induced phase separation at room temperature. The phase separation behavior and the morphological analyses of the dendritic−linear copolymer film as functions of dendritic GMA-HPAM segment contents were investigated by using AFM, TEM, and SEM. Self-assembly of the dendritic−linear PGMA-HPAM-*r*-PS copolymer in a G2−37 system containing 37 wt % of the dendritic GMA-HPAM segment, which exhibits the second generation dendron, showed submicrometer phase segregation with the main chain styrene segment. Interestingly, the submicrometer phase segregation morphology of the G2−37 sample represented a uniform size distribution of the hexagonally ordered structures. Our results prove that controlling the appropriate macromonomer content by grafting a three-dimension structure results in self-assembly and provides a honeycomb ordered microporous copolymer matrix.

Introduction

With the rapid development of synthetic chemistry, many new molecular structures can be designed to investigate the role of polymer topology on the physical and chemical properties of macromolecules in traditional, block, hyperbranch, and, in particular, dendritic copolymers. Among them, dendritic macromolecular chemistry[1−4] has recently attracted significant attention due to its various functions and the properties that result from its special structures and characteristics. Dendritic macromolecules, called dendrimers, were first successfully introduced in the mid-1980s by Tomalia, et al.[5−7] Because of their special three-dimensional structure and characteristics, dendritic macromolecules, which can be synthesized by both divergent[5] and convergent[8,9] methods, exhibit unique physical and chemical properties,[8−15] such as low intrinsic viscosity, high solubility, high miscibility, and high reactivity. Therefore, the use of dendritic segments or dendrons to construct hybrid copolymers is of significant interest to scientists.[16−18] On the basis of the structural features of the dendritic segment or dendron, dendritic hybrid copolymers can be classified as follows: dendritic−linear polymers,[19−24] dendritic−comb polymers,[27−29] and dendronized polymer−linear polymers.[30,31] The effect of the branched structure and the functionality of the dendritic segment or dendron renders the properties of the dendritic copolymers significantly different from conventional linear copolymers both in solvent and in bulk. The self-assembling structure of dendritic−linear copolymers in bulk shows that the dendritic segment affects the phase boundary and improves phase separation.[24−26] Therefore, dendritic macromolecular chemistry and physics holds promise for various applications in the field of materials science.

Microporous thin films with perfect arrangements of ordered structures (10 μm ≥ pore size ≥ 50 nm) have also garnered increased interest over the past few years, since they have great potential for use as templating materials,[32] membrane filters,[33] optical filters,[34] electronic and optical devices,[35−37] catalytic supports,[38] and biosensors.[39] The templating method and "breath figure" approach are two of the most widely used techniques for the fabrication of ordered microporous films. In the templating method, uniform spherical particles (usually silica[40] or polymer spheres[41]) are used as a template, and ordered microporous structure films are formed when the templates are removed.[42,43] Alternatively, a template-free method called the "breath figure" approach utilizes moist air flow to create microdroplets of water that work as a template for the micropores in the condensing and self-assembling block copolymer solutions. After complete evaporation of the solvent, the water droplets remain in the copolymer films, forming a perfectly ordered microporous copolymer structure.[44−49]

In this report, we demonstrate the self-assembly of the dendritic−linear copolymer, poly(glycidyl methacrylate-grafted dimethyl 3,3′-(4-hydroxyphenylazanediyl)bis(2-methylpropanoate))-*random*-polystyrene (PGMA-HPAM-*r*-PS), to create microporous films over an area of more than 2 cm^2 via solvent-induced phase separation.[50,51] We characterize the morphology of these copolymer films using transmission electron microscopy (TEM), scanning electron microscopy (SEM), and AC mode atomic force microscopy (AFM). Furthermore, we show how a hexagonally ordered microporous structure, of 1.4−1.6 μm

*To whom all correspondence and reprint requests should be addressed *E-mail address:* ccy7@ccmail.ncku.edu.tw(C.Y.Chen) Tel: +886-6-2360468; Fax: +886-6-2344496.

Published on Web 06/18/2009

micropore size, can form on the film surface of the dendritic copolymer. We investigate the influence of the weight ratio of the dendritic segment to the dendritic−linear copolymer system on the number of ordered/disordered states, the number density of micropores, and the uniformity of the micropore size. We demonstrate that this experimental process is significantly different from the mechanism of microporous formation under moist air flow conditions.

Experimental Section

Materials. Reagents were purchased from Aldrich and Fluka Co., Ltd., and used without further purification unless otherwise indicated. *p*-Aminophenol and ethylenediamine (EDA) were used as received. Styrene, methyl methacrylate (MMA), and glycidyl methacrylate (GMA) (Merck Co., Ltd.) were purified by using a distillation method under reduced pressure. They were stored at 5 °C before use.

Polymerization Procedure for the Dendritic−Linear Copolymer. *I. Synthesis of Dimethyl 3,3′-(4-(2-Hydroxy-3-(methacryloyloxy) propoxy)phenylazanediyl)bis(2-methylpropanoate) (GMA-HPAM) Macromonomer*. We first synthesized the dendron 3,3′-(4-hydroxyphenylazanediyl)bis(*N*-(2-aminoethyl)-2-methylpropanamide) (HPAM). A solution of freshly distilled MMA in methanol was added dropwise to the solution of *p*-aminophenol in methanol under nitrogen over 2 h. The final mixture was stirred for 1 h at 0 °C, allowed to come to room temperature, and further stirred for 5 days. The solvent was removed under reduced pressure at 40 °C by using a rotary evaporator, and the resulting reddish-brown oil was dried in a vacuum oven overnight to yield the final product (G1). FT-IR υ_{max}/cm^{-1}: 1740 (C═O). ^{1}H NMR ($CDCl_3$, TMS, δ_H, ppm): 1.26 (t, 6H, −C***H***$_3$), 2.58 (s, 2H, −CH$_2$−C***H***(−CH$_3$)−C(═O)−O), 2.81 (m, 4H, Ar−N(−CH$_2$−)−C***H***$_2$−CH−), 3.62 (m, 6H, C(═O)−O−C***H***$_3$), 6.55 and 6.71 (m, 4H, −O−Ar***H***−N−).

A solution of G1 precursor in methanol was carefully added to a vigorously stirred solution of ethylenediamine in an ice bath at 0 °C and stirred for 5 days at room temperature. The solvent was removed under reduced pressure at 40 °C, and the excess ethylenediamine was removed by using toluene extraction. Finally, we obtained the amine-terminated product (G1.5), which is a reddish-brown oil. FT-IR υ_{max}/cm^{-1}: 1658 (C═O), 3200 (NH$_2$), 3400 (NH). ^{1}H NMR ($CDCl_3$, TMS, δ_H, ppm): 1.26 (t, 6H, −C***H***$_3$), 2.19 (m, 4H, −CH$_2$−CH$_2$−N***H***$_2$), 2.57 (s, 2H, −CH$_2$−C***H***(−CH$_3$)−CO−O−), 2.60 (m, 4H, −NH−CH$_2$−C***H***$_2$−NH$_2$), 2.81 (m, 4H, Ar−N(−CH$_2$−)−C***H***$_2$-CH−), 2.88 (m, 4H, −CO−NH−CH$_2$−C***H***$_2$−), 6.63 and 6.81 (m, 4H, −O−Ar***H***−N−), 6.97 (s, 2H, −CO−N***H***−CH$_2$−).

The designed higher generational product of the HPAM dendron was obtained by repeating the previous procedure.

Subsequently, the solution of the G2-HPAM dendron in N, N-dimethylacetamide was carefully added to the vigorously stirred solution of glycidyl methacrylate (GMA) at 0 °C. The final mixture was stirred for 30 min at 0 °C and then further stirred for 12 h at room temperature. The excess G2 HPAM dendron was removed using extraction by methanol, and we then obtained the dendritic macromonomer of the GMA-HPAM, a transparent orange oil. FT-IR υ_{max}/cm^{-1}: 1640 (C═C), 1658 (C═O), 1740 (C═O). ^{1}H NMR ($CDCl_3$, TMS, δ_H, ppm): 1.28 (m, 18H, −CH$_2$−CH−C***H***$_3$), 1.84 (s, 3H, −C═C(−C***H***$_3$)−CO−), 2.48 and 2.92 (s, 8H, −CH$_2$−N(−C***H***$_2$−)−C***H***$_2$−CH−), 2.63 (m, 4H, −NH−CH$_2$−C***H***$_2$−N−), 2.78 (s, 2H, −CH$_2$−C***H***(−CH$_3$)−C(═O)−), 2.92 (m, 4H, −CH$_2$−C***H***−CO−), 3.35 (m, 4H, −NH−C***H***$_2$−CH$_2$−), 3.69 (m, 12H, −CO−O−C***H***$_3$), 3.81 (m, 4H, Ar−N−C***H***$_2$−CH−), 4.11(m, 2H, Ar−O−C***H***$_2$−CH−), 4.35 (m, 1H, −CH$_2$−C***H***(−OH)−CH$_2$−), 4.59 (m, 2H, −O−C***H***$_2$−CH(−OH)−), 5.78 and 6.05 (m, 3H, C***H***$_2$═C***H***−), 6.49 (m, 4H, −O−Ar***H***−N−), 6.83 (s, 2H, −CO−N***H***−CH$_2$−).

II. Synthesis of the Dendritic−Linear Copolymer. A solution of the GMA-HPAM macromonomer in *N*,*N*-dimethylacetamide was added dropwise to a three-neck 250 mL round-bottom flask under nitrogen, which contained the mixed solution of initiator, azobisisobutyronitrile (AIBN), and styrene monomer in *N*,*N*-dimethylacetamide. The final mixture was stirred for 1 h at room temperature and then heated to 80 °C with stirring for 48 h. Finally, the dendritic−linear copolymers (PGMA-HPAM-*r*-PS) were precipitated in methanol solution, separated by filtration, and dried in a vacuum oven. ^{1}H NMR ($CDCl_3$, TMS, δ_H, ppm): 0.50−3.38 (m, −C***H***−, −C***H***$_2$−, −C***H***$_3$), 3.69 (m, 12H, −CO−O−C***H***$_3$), 3.90−4.2 (m, 5H, −O−C***H***$_2$−C***H***(−OH)−C***H***$_2$−O−Ar), 6.65−7.37 (m, 9H, ***benzene***), 7.08 (m, 1H, −CO−N***H***−).

III. Preparation of the PGMA-HPAM-r-PS Copolymer Films. Microporous films were prepared by casting the 30 wt % PGMA-HPAM-*r*-PS copolymer solution in THF at room temperature in a glovebox under a nitrogen atmosphere onto a variety of substrates, such as glass slides, aluminum plates, metal wafers, and mica.

Characterization. The molecular weight of the raw sample and its distribution were determined by gel permeation chromatography (GPC) including of Postnova 1021 solvent delivery pump, Viscotek 270 dual detector, Viscotek VE 3580 RI detector, and American Polymer Standards Corporation 10 μm AM Gel GPC columns (AM Gel 10^3Å, 10^4Å, and 10^5Å) with linear polystyrene (PS) standards. Tetrahydrofuran (HPLC grade) was used as the eluent, and the flow rate was set to 0.7 mL/min. ^{1}H NMR and ^{13}C NMR spectra were recorded with a Bruker 400-MHz FT-NMR instrument, and the chemical shifts were recorded in parts per million with tetramethylsilane as an internal standard. Fourier transfer infrared (FT-IR) spectra were recorded with a Varian 2000 FT-IR analyzer, which scanned from 700 to 4000 cm^{-1} at room temperature. Spectra were obtained using a resolution of 4 cm^{-1}, and were averaged over 32 scans in pellet samples. A Hitachi model HF-2000 field emission transmission electron microscope (TEM) and a JEOL JSM-6700F high resolution field emission scanning electron microscope (HRFE−SEM) were used to observe the morphology of the dendritic−linear PGMA-HPAM-*r*-PS copolymer. An Agilent 5500 AC (dynamic) mode atomic force microscope (TM−AFM) was used to observe the level and phase morphology of the dendritic−linear PGMA-HPAM-*r*-PS copolymer.

Results and Discussion

Synthesis and Characterization. Figure 1 shows the ^{1}H NMR and ^{13}C NMR spectra for the dendritic−linear PGMA-HPAM-*r*-PS copolymer. ^{1}H NMR was used to determine the content of the dendritic GMA-HPAM segment for the dendritic−linear PGMA-HPAM-*r*-PS copolymer through a comparison of the peak integration values. Specifically, the integration value from the dendritic GMA-HPAM segment ester group (−CO−OC***H***$_3$), which appeared around 3.69 ppm, was compared with the integration values from the proton of the amide group (−CO−N***H***−) spectra in the dendritic GMA-HPAM segment, which appeared at 7.08 ppm, and with the phenyl group spectrum of the styrene segment and the dendritic GMA-HPAM segment, which appeared at 6.6−7.4 ppm. On the basis of the calculated results, the dendritic−linear PGMA-HPAM-*r*-PS copolymers were defined as G2−*X*, where *X* represents the weight percentage of the dendritic GMA-HPAM segment in PGMA-HPAM-*r*-PS copolymers. Therefore, G2−9 represents the second generation dendron in each dendritic segment, and it occupies 9 wt % of the whole dendritic−linear PGMA-HPAM-*r*-PS copolymer. The series of percentages in this research include G2−9, G2−14, G2−21, G2−27, G2−37, G2−41, G2−49, and G2−58. From the ^{13}C NMR analysis in Figure 1b, the signal at 38 ppm, namely the main chain −C−C− bonds of the styrene segment, can manifest

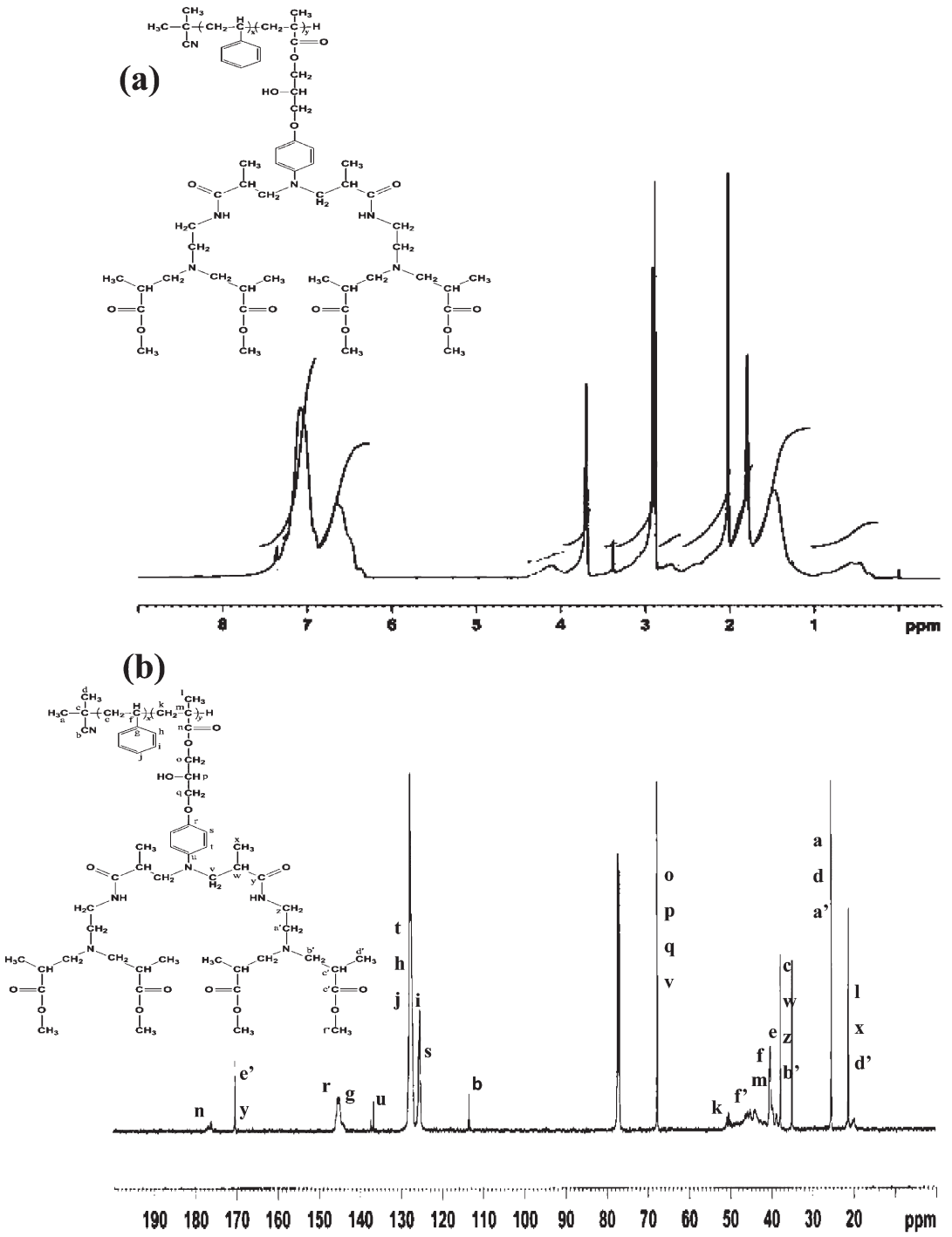

Figure 1. (a) ^{1}H NMR and (b) ^{13}C NMR spectrum of the dendritic−linear PGMA-HPAM-*r*-PS copolymer in $CDCl_3$.

the formation of the PGMA-HPAM-*r*-PS copolymer. In addition to the ^{13}C NMR spectrum of the PGMA-HPAM-*r*-PS copolymer shown in Figure 1b, the dendritic−linear PGMA-HPAM-*r*-PS copolymers were successfully synthesized in this study. For each G2−*X* copolymer, its generation number, molecular weight, weight percentage of the dendritic GMA-HPAM segment, and PDI are listed in Table 1.

Polymer Morphology. Figure 2 shows the typical TEM images for various weight percentages of the dendritic segment in the dendritic−linear PGMA-HPAM-*r*-PS copolymer formed at room temperature. Those samples were stained by OsO_4 vapor in a close chamber for 8 h before TEM measurement. While OsO_4 reacts with both segments of the dendritic−linear PGMA-HPAM-*r*-PS copolymer, the dendritic GMA-HPAM segment was stained stronger than the main chain of the styrene segment, thus providing significant electron density contrast. Consequently, the dendritic GMA-HPAM segment domains in these images appear as dark globules, which were formed by a group of large irregular aggregate clusters or superstructures. The aggregates formed in aqueous solution are spherical and range from 30 to 90 nm in diameter. The dendritic GMA-HPAM segment clusters of the dendritic−linear PGMA-HPAM-*r*-PS copolymer from several molecules must aggregate together to form the smaller domains of 30−50 nm in diameter, as indicated by their size relative to the individual dendritic GMA-HPAM segment. The dendron size for generation 1.0 is about 0.7 nm, the dendron size for generation 2.0 is about 1

Table 1. PGMA-HPAM-*r*-PS Molecular Characteristics and Morphology

designation (generation no.−GMA-HPAM segment wt %)	dendron	GMA-HPAM-segment wt %	M_w (10^3g/mol)	PDI	morphology (SEM)
2−9	G2	8.8	44.8	1.459	phase separation/disordered
2−14	G2	13.9	26.7	1.713	phase separation/disordered
2−21	G2	21.4	32.4	1.584	phase separation/pseudo-disordered
2−27	G2	26.8	28.9	1.674	phase separation/honeycomb-ordered
2−37	G2	36.9	36.7	1.576	phase separation/pseudo-ordered
2−41	G2	41.4	38.5	1.672	phase separation/disordered
2−49	G2	49.3	42.2	1.944	phase separation/disordered
2−58	G2	57.8	47.5	1.832	phase separation/disordered
3−33	G3	33.2	26.1	1.751	phase separation/honeycomb-ordered

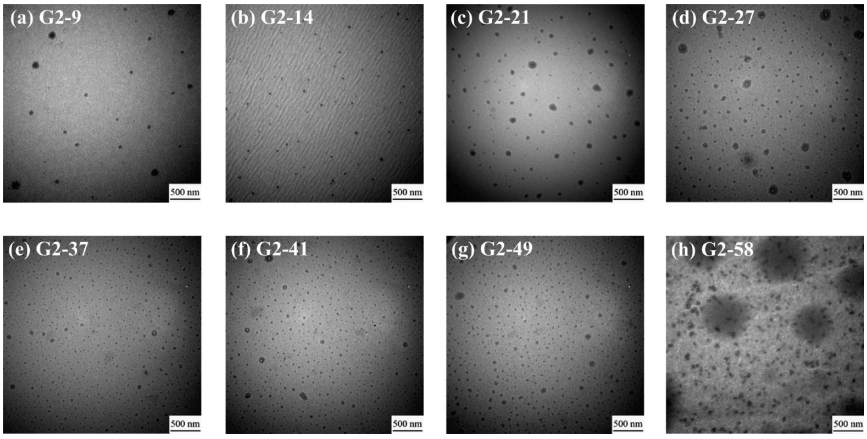

Figure 2. TEM photographs of the PGMA-HPAM-*r*-PS copolymers with different dendritic GMA-HPAM segment contents. The dark-colored regions correspond to the dendritic GMA-HPAM segment in copolymer stained by OsO_4. Key: (a) G2−9, (b) G2−14, (c) G2−21, (d) G2−27, (e) G2−37, (f) G2−41, (g) G2−49, and (c) G2−58.

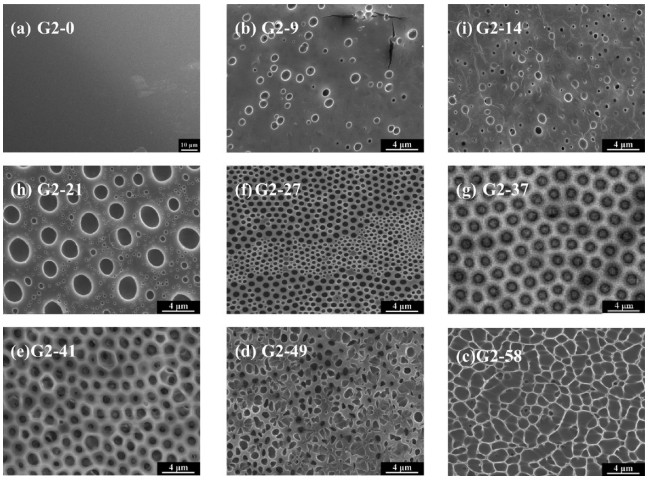

Figure 3. SEM photographs of the microporous PGMA-HPAM-*r*-PS copolymer film given different dendritic GMA-HPAM segment contents. Key: (a) G2−0, (b) G2−9, (c) G2−14, (d) G2−21, (e) G2−27, (f) G2−37, (g) G2−41, (h) G2−49, and (i) G2−58.

nm, and the dendron size for generation 3.0 is about 1.5 nm.[52−54] However, it is also possible that the staining of the dendritic GMA-HPAM segment by OsO_4 results in structures that are larger than their actual size. Surrounding the aggregated zones are the styrene segment domains. Many isolated dendritic GMA-HPAM segments are apparent as small dark gray dots of approximately 30 nm or less within the styrene segment domains. This result is attributed to the mobility and aggregation of the dendritic GMA-HPAM segments under the influence of the main chain of the dendritic−linear PGMA-HPAM-*r*-PS copolymer.

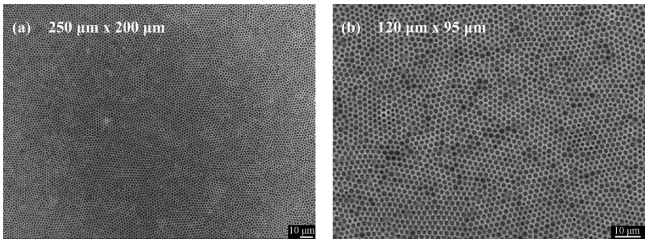

Figure 4. SEM photographs of the hexagonally ordered microporous matrix of the PGMA-HPAM-*r*-PS G2−37 copolymer at larger length scales. Key: (a) 250 μm × 200 μm; (b) 120 μm × 95 μm.

Furthermore, the dendritic−linear PGMA-HPAM-*r*-PS copolymer microporous films were prepared at room temperature by casting the THF solution onto the substrate. A series of SEM photographs of films with different weight percentages of the dendritic GMA-HPAM segment in the dendritic−linear PGMA-HPAM-*r*-PS copolymers are shown in Figure 3. From these photographs, we see that the size, area, and arrangement of micropores tend to increase with greater dendritic GMA-HPAM segment content. In particular, the formation of hexagonally packed micropores with a uniform size distribution was clearly observed in the SEM image of the G2−37 film in Figure 3. Even on larger length scales of 250 μm × 200 and 120 μm × 95 μm of the SEM photographs of G2−37 in Figure 4, we still observed that the dendritic GMA-HPAM segment microphase can readily separate from the PS block matrix, revealing a hexagonally ordered structure. In addition, Figure 5 shows AFM images of 7 μm × 7 and 100 μm × 100 μm scans of the G2−37 sample. The

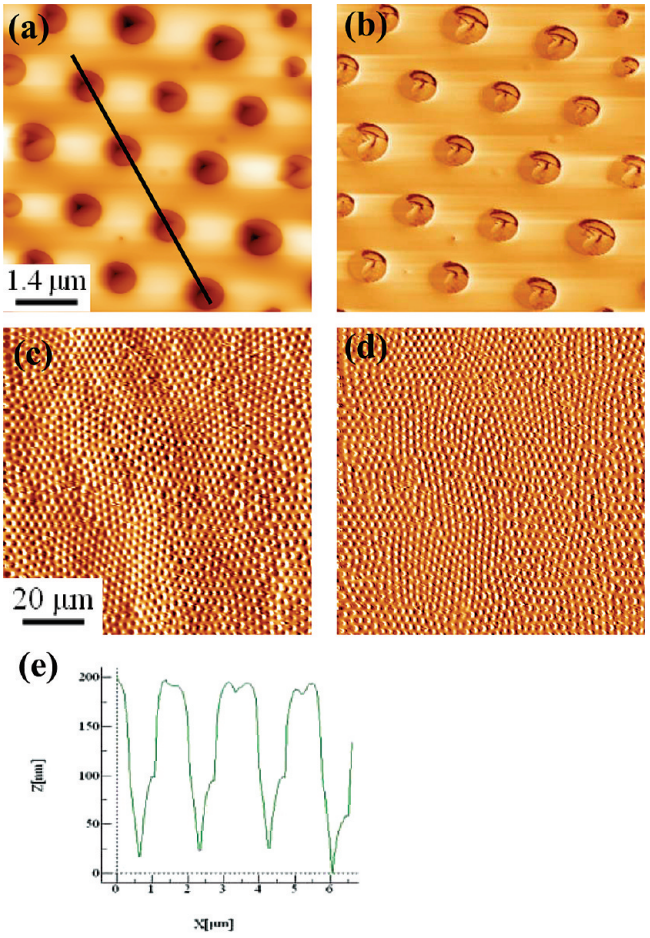

Figure 5. AFM photographs of the PGMA-HPAM-*r*-PS G2−37 copolymer matrix. Key: (a) topography diagram (7 μm × 7 μm), (b) phase diagram (7 μm × 7 μm), (c) topography diagram (100 μm × 100 μm), (d) phase diagram (7 μm × 7 μm), and (e) the level of the selected line in part a.

ordered micropores are all oriented perpendicular to the surfaces. According to the SEM and AFM photographs, the average diameters of the self-assembly micropores were estimated to be from 1.4 to 1.6 μm. The depth of the micropores is approximately 400 nm, as shown in Figure 5c (the selected line in Figure 5a). Furthermore, the average interval distance of the hexagonally ordered structures in the SEM and AFM images were found to be from 1.8 to 2 μm. From these results, one can calculate the volumetric fraction of the hexagonally ordered structures in the dendritic−linear PGMA-HPAM-*r*-PS film. According to reports in the literature, the relation between volumetric fraction (φ), radius (R), and repeating distance (L) the hexagonally ordered cylinders is given by[55,56]

$$\varphi = \frac{2}{3}\pi\sqrt{3}\left(\frac{R}{L}\right)^2$$

Considering that L = 1.8−2 μm and R = 0.7−0.8 μm, the volumetric fraction of the micropores φ is 0.55 to 0.58. The dendron is a three-dimensional architecture, and its configuration can be extended by a wide margin. This may explain the high values of the volumetric fraction obtained by G2−37. Consequently, we surmise that the micropores in the self-assembly film matrix are made by the aggregate of the dendritic GMA-HPAM segment of the dendritic−linear PGMA-HPAM-*r*-PS copolymer.

In order to further confirm the aforementioned assumption, we employed staining technology to observe the morphology of the dendritic−linear PGMA-HPAM-*r*-PS copolymer films. Figure 6 shows SEM images of the self-assembly honeycomb G2−37 films prepared by the same procedure and stained/unstained by OsO_4. Figure 6b illustrates the film of the dendritic GMA-HPAM segment of the G2−37 copolymer that was stained by OsO_4. Compared with the unstained version (Figure 6a), the stained domains of the dendritic−linear PGMA-HPAM-*r*-PS copolymer G2−37 show small bright spots with sizes that are consistent with the morphology of the TEM images. Under greater magnification, one can observe the aforementioned phenomenon in greater detail, revealing a significant difference between parts c and d of Figure 6. In addition, parts e and f of Figure 6 show the EDS spectrum of the micropores in G2−37 copolymer films (the region selected in Figure 6, parts a and b). Compared with the unstained G2−37 micropore film, the stained G2−37 micropore film shows new peaks of Os components. The peak of Os becomes more pronounced, a change that can be attributed to the OsO_4 stained with the dendritic GMA-HPAM segment of the G2−37 copolymer. Therefore, these results prove that the micropores are formed by the aggregation of the dendritic GMA-HPAM segment in the dendritic−linear PGMA-HPAM-*r*-PS copolymer. The type of microporous structure is determined by the dendritic GMA-HPAM segment content of the dendritic−linear PS copolymer.

Formation Mechanism of the Ordered/Disordered Microporous Surface Structure. Scheme 1 illustrates the formation mechanism of the hexagonal ordered micropore morphology via self-assembly. In copolymer solution, different segments can aggregate micelles of different sizes and shapes. Therefore, the continuous or dispersed condition of each styrene and dendritic segment will control the surface morphology of the dendritic−linear copolymer films. In our case, because the entanglement and mobility of the dendritic GMA-HPAM segment are constrained by the main chain in the PGMA-HPAM-*r*-PS copolymer, the shapes and volumes of the dendritic GMA-HPAM segment micelle domains are related to the styrene segment domains in solution. The dendritic GMA-HPAM segment domains should prefer to form spherical shapes following the thermodynamic behavior because the styrene segment contents are much larger than the dendritic segment; thus, the PGMA-HPAM-*r*-PS copolymer films that exhibit a spherical microporous matrix are formed after solvent evaporation in SEM images (Figure 2). With several different dendritic segment contents, the styrene segments in the copolymer account for the majority of the continuous phase, and the dendritic segments are compressed into small particle micelles that are dispersed in the styrene phase. Therefore, the micropores formed by the dendritic segments are highly dispersed on copolymer film surfaces like G2−9 and G2−14 (Figure 3, parts b and c). Under this condition, the morphology of the copolymer films is controlled by the continuous phase of the styrene segment in the copolymers (route A in Scheme 1).

With increasing the dendritic segment content, the micelle volumes of the dendritic segments increase significantly. However, they are not large enough to affect the continuous phase morphology of the styrene segments in the copolymer. Therefore, nonuniform micropore sizes can be seen on a copolymer film surface like G2−21 (Figure 3d), and in this case the morphology is still controlled by the styrene segment in copolymers (route B in Scheme 1).

With further increase in the dendritic segment content in the copolymer, each micelle begins to cause a pseudo-ordered

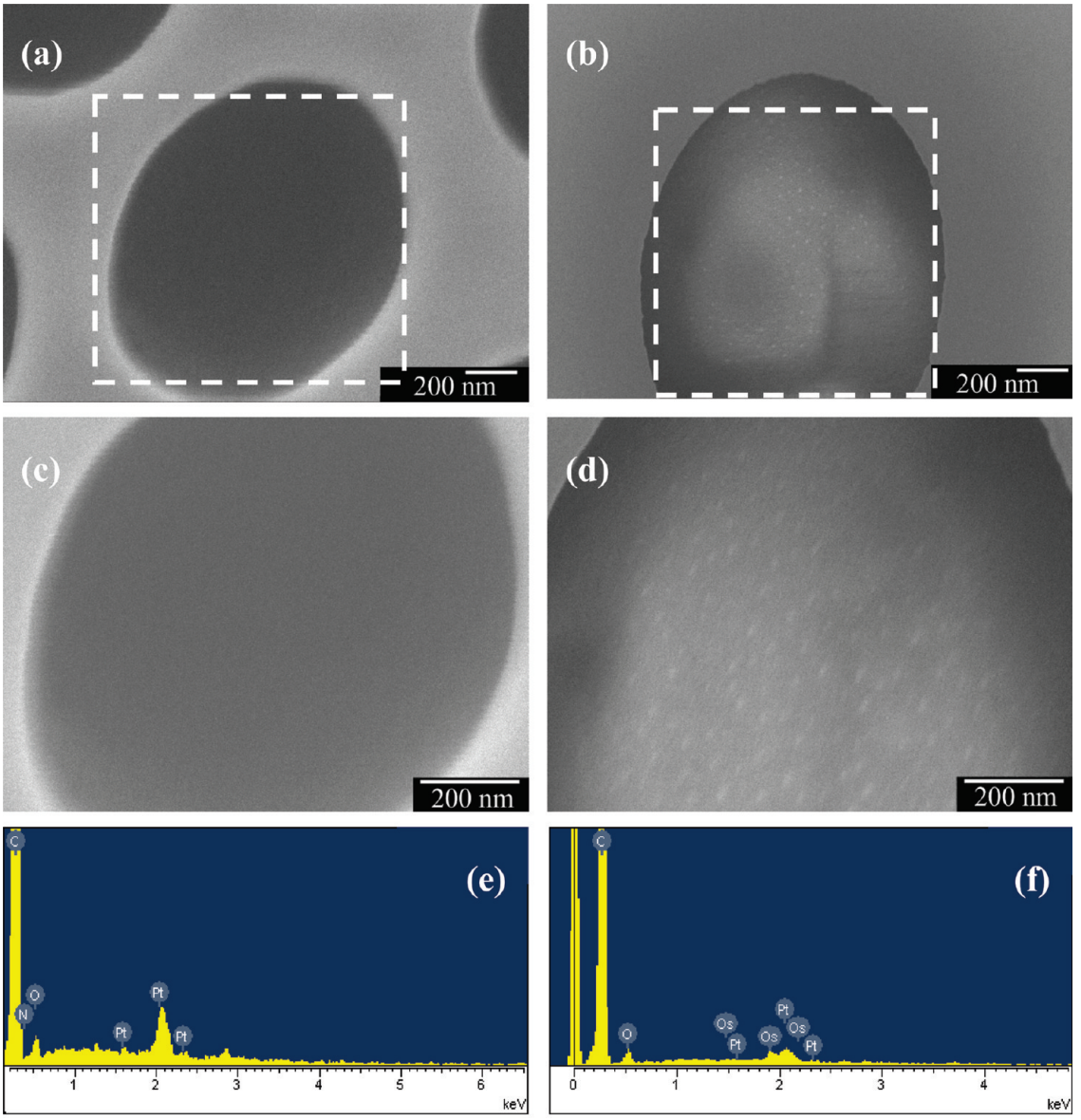

Figure 6. SEM photographs of the hexagonally ordered microporous G2−37 matrix. Key: (a) unstained, (b) stained by OsO_4, (c) a larger scanning image of part a, (d) a larger scanning image of part b, (e) EDS spectrum of selected region in part a, and (f) EDS spectrum of selected region in part b.

condition like G2−27 (Figure 3e) due to the inter- and intra-action of the styrene and the dendritic segment. Moreover, there exists a hexagonally ordered structure on the copolymer film surfaces when the dendritic segment contents approximately reach a critical equilibrium like G2−37 (Figure 3f). Afterward, the balance between the micelles of each segment is slightly disrupted, leading to a pseudo-ordered condition like G2−41 (Figure 3g). The surface morphology is gradually affected by the dendritic segment micelles under this condition (route C in Scheme 1).

When the morphology of the dendritic segment in the copolymer forms a continuous phase, the continuous and dispersed phases of the styrene segments appear in these systems, as with G2−49 and G2−58 (Figure 3, parts h and i). Therefore, the disordered morphology of continuous and dispersed phases due to each kind of segment is formed on the copolymer matrix surface. The surface information is jointly controlled by the styrene and the dendritic segments (route D in Scheme 1).

Generally, block copolymer micelle formation is controlled by the properties of and interactions between each segment, but it is difficult to order the domain because of the interactions between each segment with the same or different copolymer in solution. In our case, a high degree of extension and the three-dimensional structure of the dendron can establish and influence the process of copolymer micelle domain formation in solution. For this reason, the volumetric fraction is close to 60% in the G2−37 hexagonally ordered system. In addition, synthesis and control of dendritic macromonomer polymerization is much easier than the dendritic macroinitiator polymerization, since it is only necessary to control the weight percentage of the dendritic GMA-HPAM segment to what is needed to achieve the desired objectives in our system. Many studies have discussed the structure of three-dimensional films and submicrometer films by means of the water-assisted method. According to their results, the ordered structures are formed by evaporating systems of the rod−coil block copolymers in a volatile solvent in the presence of moisture with forced airflow across the solution surface. The water vapor condenses into droplets on the polymer solution surface because the high vapor pressure of the solvent and the velocity of the humid airflow across the surface drive solvent evaporation, rapidly

Scheme 1. Formation Mechanism of the Ordered/Disordered Micropores on the Surface of the PGMA-HPAM-*r*-PS Copolymer Films

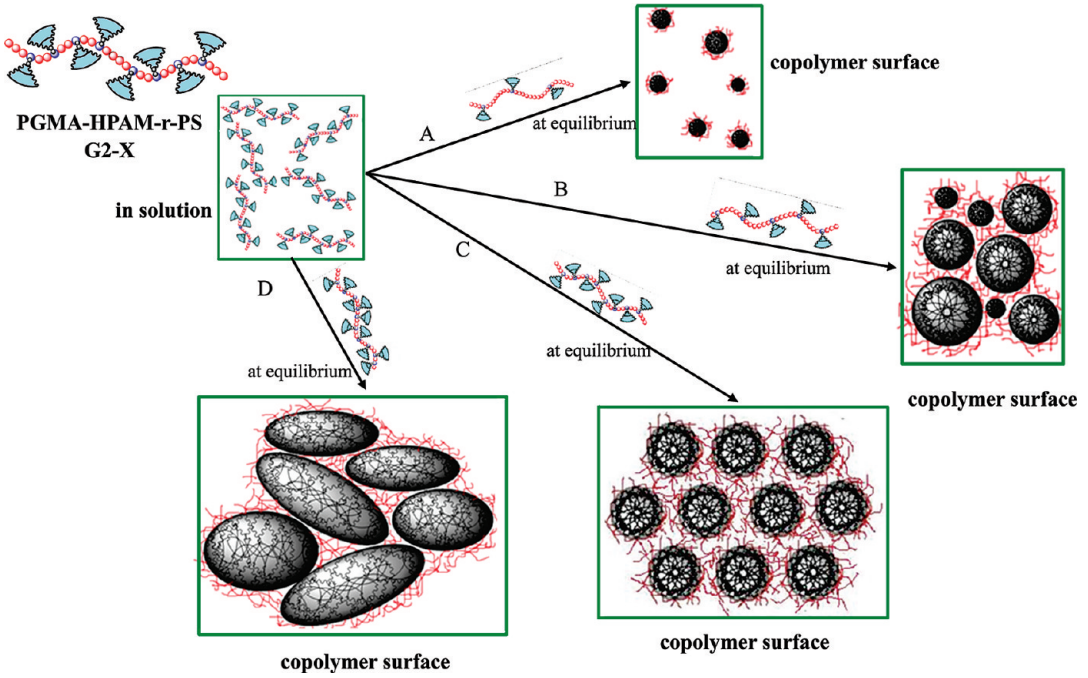

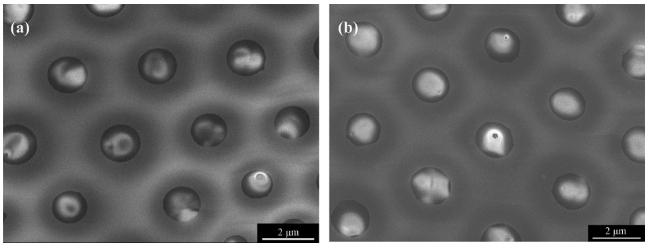

Figure 7. SEM photographs of the hexagonally ordered microporous matrix for (a) G2−37 and (b) G3−31 copolymer stained by OsO_4.

cooling the surface. This cooling leads to the nucleation and growth of water droplets as a function of time, following which the condensing water droplets form a hexagonally packed array on the solution surface. The evaporation of the solvent and the water creates the three-dimensional ordered porous architecture. The size of the pores formed under the water-assisted method is influenced by several key factors, such as the properties of the block copolymer and the relative humidity and airflow velocity. Film preparation is challenging because of the need for a special block copolymer polymerization treatment. Therefore, our research results suggest a new, simple, and direct route to construct the honeycomb microporous matrix by means of self-assembly.

In summary, this study shows that honeycomb microporous structures can form not only from the second generation of the dendritic GMA-HPAM segment in the dendritic−linear PGMA-HPAM-*r*-PS G2−37 but also from the third generation PGMA-HPAM-*r*-PS G3−33 copolymer (Figure 7). The pore size of the uniform distribution G3−33 copolymer was observed to be approximately 1.7−2.0 μm, still maintaining a high micropore volumetric fraction, with φ = 0.41 to 0.46.

Conclusion

We prepared dendritic−linear PGMA-HPAM-*r*-PS copolymers by simple and direct polymerization with the dendritic GMA-HPAM macromonomer and a styrene monomer. The microporous structure films were successfully manufactured by casting the PGMA-HPAM-*r*-PS copolymers using a THF solution at room temperature. The dendritic GMA-HPAM segment was shown to form spherical micelles during solvent evaporation, and we demonstrated that the volume of the dendritic GMA-HPAM micelle domain increases with the weight percentage of the dendritic GMA-HPAM segment in the copolymer. In particular, at 37 wt % of the dendritic GMA-HPAM segment in the G2−37 copolymer, the dendritic segment micelle displayed self-assembling behavior, resulting in a hexagonally ordered microporous copolymer matrix. Our research confirms that controlling the appropriate macromonomer content by grafting a three-dimensional structure can promote self-assembly and provides a honeycomb ordered microporous copolymer matrix.

Acknowledgment. We gratefully acknowledge the financial support of the Ministry of Economic Affairs of the Republic of China (TDPA: 95-EC-17-A-05-S1-0014) and the National Science Council (NSC: 96-2221-E-006-100-MY3).

References and Notes

(1) Tomalia, D. A. *Macromol. Symp.* **1996**, *101*, 243.
(2) Tomalia, D. A.; Brothers , H. M., II; Piehler, L. T.; Hsu, Y. *Polym. Mater. Sci. Eng* **1995**, *73*, 75.
(3) Dvornic, P. R.; Tomalia, D. A. *Science Spectra* **1996**, *5*, 36.
(4) Naj, A. K. *Persistent Inventor Markets a Molecule. Wall Street J.*, 1996; p B1.
(5) Tomalia, D. A.; Baker, H.; Dewald, J.; Hall, M.; Kallos, G.; Martin, S.; Roeck, J.; Ryder, J.; Smith, P. *Polym. J. (Tokyo)* **1985**, *17*, 117.
(6) Tomalia, D. A.; Baker, H.; Dewald, J.; Hall, M.; Kallos, G.; Martin, S.; Roeck, J.; Ryder, J.; Smith, P. *Macromolecules* **1986**, *19*, 2466.
(7) Tomalia, D. A., Dewald, T. R. *US Pat. 4,568,737*, 1986.
(8) Fréchet, J. M. J.; Hawker, C. J. *J. Am. Chem. Soc.* **1990**, *112*, 7638.
(9) Grayson, S. M.; Fréchet, J. M. J. *Chem. Rev.* **2001**, *101* (12), 3819.
(10) Fréchet, J. M. J.; Hawker, C. J.; Gitsov, I.; Leon, J. W. *J. Macromol. Sci. Pure* **1996**, *A33*, 1399.
(11) Fréchet, J. M. J. *Science* **1994**, *263*, 1710.
(12) Wooley, K. L.; Hawker, C. J.; Lee, R.; Fréchet, J. M. J. *Polym. J.* **1994**, *26*, 187.
(13) Gitsov, I.; Wooley, K. L.; Hawker, C. J.; Ivancva, P. T.; Fréchet, J. M. J. *Macromolecules* **1993**, *26*, 5621.

(14) Tomalia, D. A.; Dupont-Durst, H. *J. Chem. Soc., Perkin Trans. 1* **1993**, 1287.
(15) Mourey, T. H.; Turner, S. R.; Rubinstein, M.; Fréchet, J. M. J.; Hawker, C. J.; Wooley, K. L. *Macromolecules* **1992**, *25*, 2401.
(16) Cheng, C. X.; Jiao, T. F.; Tang, R. P.; Chen, E. Q.; Liu, M. H.; Xi, F. *Macromolecules* **2006**, *39*, 6327.
(17) Percec, V.; Dulcey, A. E.; Peterca, M.; Ilies, M.; Sienkowska. M. J.; Heiney, P. A. *J. Am. Chem. Soc.* **2005**, *127*, 17902.
(18) Schluter, A. D.; Rabe, J. P. *Angew. Chem., Int. Ed.* **2000**, *39*, 864.
(19) Leduc, M. R.; Hawker, C. J.; Dao, J. L.; Fréchet, J. M. J. *J. Am. Chem. Soc.* **1996**, *118*, 11111.
(20) Gillies, E. R.; Jonsson, T. B.; Fréchet, J. M. J. *J. Am. Chem. Soc.* **2004**, *126*, 11936.
(21) Yoo, Y. S.; Choi, J. H.; Oh, N. K.; Zin, W. C.; Park, S.; Chang, T.; Lee, M.; Cho, B. K. *J. Am. Chem. Soc.* **2004**, *126*, 6294.
(22) Kim, Y. S.; Gil, E. S.; Lowe, T. L. *Macromolecules* **2006**, *39*, 7805.
(23) Cheng, C. X.; Tian, Y.; Shi, Y. Q.; Tang, R. P.; Xi, F. *Langmuir* **2005**, *21*, 6576.
(24) Mackay, M. E.; Hong, Y.; Jeong, M.; Tande, B. M.; Wagner, N. J.; Hong, S.; Gido, S. P.; Vestberg, R.; Hawker, C. J. *Macromolecules* **2002**, *35*, 8391.
(25) Jung, H.-T.; Kim, S. O.; Ko, Y. K.; Yoon, D. K.; Hudson, S. D.; Percec, V.; Holerca, M. N.; Cho, W.-D.; Mosier, P. E. *Macromolecules* **2002**, *35*, 3717.
(26) Mezzenga, R.; Ruokolainen, J.; Canilho, N.; Kasemi, E.; Schluter, D. A.; Lee, W. B.; Fredrickson, G. H. *Soft Matter* **2009**, *5*, 95.
(27) Tian, L.; Hammond, P. T. *Chem. Mater.* **2006**, *18*, 3976.
(28) Tian, L.; Hammond, P. T. *Chem. Commum.* **2006**, 3489.
(29) Percec, V.; Peterca, M.; Dulcey, A. E.; Imam, M. R.; Hudson, S. D.; Nummelin, S.; Adelman, P.; Heiney, P. A. *J. Am. Chem. Soc.* **2008**, *130*, 13079.
(30) Sanitini, C. M. B.; Johnson, M. A.; Boedicker, J. Q.; Hatton, T. A.; Hammond, P. T. *J. Polym. Sci., Part A* **2004**, *42*, 2784.
(31) Sanitini, C. M. B.; Hatton, T. A.; Hammond, P. T. *Langmuir* **2006**, *22*, 7487.
(32) Yabu, H.; Shimomura, M. *Langmuir* **2005**, *21*, 1709.
(33) Ballew, H. W. *Am. Biotechnol. Lab.* **1997**, *May*, 8
(34) Gupta, S.; Tuttle, G.; Sigalas, M.; Ho, K. M. *Appl. Phys. Lett.* **1997**, *71*, 2412.
(35) Judith, E. G.; Wijnhoven, J.; Willem, L. V. *Science* **1998**, *281*, 802.
(36) Muller, M.; Zentel, R.; Maka, T.; Romanov, S. G.; Torres, C. M. S. *Adv. Mater.* **2000**, *12*, 1499.
(37) Fichet, G.; Cororan, N.; Ho, P. K. H.; Arias, A. C.; MacKenzie, J. D.; Huck, W. T. S.; Friend, R. H. *Adv. Mater.* **2004**, *16*, 1908.
(38) Deleuze, H.; Schultze, X.; Sherrington, D. C. *Polymer* **1998**, *39*, 6109.
(39) Kasemo, B. *Surf. Sci.* **2002**, *500*, 656.
(40) Oberdisse, J.; Deme, B. *Macromolecules* **2002**, *35*, 4397.
(41) Mayer, A. B. R.; Grebner, W.; Wannemacher, R. *J. Phys. Chem. B* **2000**, *104*, 7278.
(42) Galloro, J.; Ginzbug, M.; MÍgues, H.; Yang, S. M.; Coombs, N.; Safa-Sefat, A.; Greedan, J. E.; Manners, I.; Ozin, G. A. *Adv. Funct. Mater.* **2002**, *12*, 382.
(43) Hong, J. C.; Park, J. H.; Chun, C.; Kim, D. Y. *Adv. Funct. Mater.* **2007**, *17*, 2462.
(44) Widawski, G.; Rawiso, M.; Francois, B. *Nature* **1994**, *369*, 387.
(45) Jenekhe, S. A.; Chen, X. L. *Science* **1999**, *283*, 372.
(46) Srinivasarao, M.; Collings, D.; Philips, A.; Patel, S. *Science* **2001**, *292*, 79.
(47) Song, L.; Bly, R. K.; Wilson, J. N.; Bakbak, S.; Park, J. O.; Srinivasarao, M.; Bunz, U. H. F. *Adv. Mater.* **2004**, *16*, 115.
(48) Zhang, Y.; Wang, C. *Adv. Mater.* **2007**, *19*, 913.
(49) Stenzel, M. H.; Kowollik, C. B., Davis, T. P. *J. Polym. Sci., Part A* **2006**, *44*, 2363.
(50) Tercjak, A.; Serrano, E.; Garcia, I.; Ocando, C.; Mondragon, I. *Acta Mater.* **2007**, *55*, 6436.
(51) Ishizu, K.; Tokuno, Y.; Makino, M. *Macromolecules* **2007**, *40*, 763.
(52) Tomalia, D. A.; Berry, V.; Hall, M.; Hedstrand, D. M. *Macromolecules* **1987**, *20*, 1164.
(53) Stechemsser, S.; Eimer, W. *Macromolecules* **1997**, *30*, 2204.
(54) Johnson, M. A.; Lyer, J.; Hammond, P. T. *Macromolecules* **2004**, *37*, 2490.
(55) Helfand, E. *Macromolecules* **1975**, *8*, 552.
(56) Van Dijk M. A.; Van den Berg R. *Macromolecules* **1995**, *28*, 6773.